Analytical and Bioanalytical Chemistry (2022) 414:3349–3358
https://doi.org/10.1007/s00216-022-03950-7

RESEARCH PAPER

A new dynamic deep learning noise elimination method for chip-based real-time PCR

Beini Zhang[1] · Yiteng Liu[2] · Qi Song[3] · Bo Li[4] · Xuee Chen[3] · Xiao Luo[3] · Weijia Wen[1,3]

Received: 31 October 2021 / Revised: 17 December 2021 / Accepted: 1 February 2022 / Published online: 2 April 2022

Abstract

Point-of-care (POC) real-time polymerase chain reaction (PCR) has become one of the most important technologies for many fields such as pathogen detection and water-quality monitoring. POC real-time PCR usually adopts chips with small-volume chambers for portability, which is more likely to produce complex noise that seriously affects the accuracy. Such complex noises are difficult to be eliminated by the traditional fixed area algorithm that is most commonly used at present because they usually have random shape, location, and brightness. To address this problem, we proposed a novel image analysis method, Dynamic Deep Learning Noise Elimination Method (DIPLOID), in this paper. Our new method could recognize and output the mask of the interference by Mask R-CNN, and then subtract the interference and select the maximum valid contiguous area for brightness analysis by dynamic programming. Compared with the traditional method, DIPLOID increased the accuracy, sensitivity, and specificity from 57.9 to 94.6%, 49.1 to 93.9%, and 65.9 to 95.2%, respectively. DIPLOID has great anti-interference, robustness, and sensitivity, which can reduce the impact of complex noise as much as possible from the aspect of the algorithm. As shown in the experiments of this paper, our method significantly improved the accuracy to over 94% under the complex noise situation, which could make the POC real-time PCR have greater potential in the future.

Keywords Deep learning · Point-of-care · PCR · Noise elimination

Introduction

With the global pandemic of the Coronavirus Disease 2019 (Covid-19), the point-of-care (POC) real-time polymerase chain reaction (PCR) that based on microfluidic chips is becoming an important detection method because of its portability and rapidity, which also has many other application scenarios such as community testing [1, 2], veterinary testing [3], and water quality detection [4]. POC PCR can greatly reduce the cost of transporting samples and allow testing, diagnosis, and treatment to be conveniently performed in the same location, which is important for controlling the spread of epidemics [5, 6]. However, because the POC real-time PCR is usually designed with small volume chambers for portability and flexibility, and the liquid often requires external power to drive and heat [7]. So it is more likely to cause pressure variation, temperature changes, and mass transport on the surface because of the limited vertical space, which may lead to a variety of interference problems such as bubbles, self-luminous debris, and light spots [8, 9]. The bubble problem is one of the most critical factors affecting the accuracy of the PCR because it not only influences the brightness value of a large area [10] but also may lead to a series of problems such as liquid leakage and evaporation, so it may increase the probability of producing other complex noises [8]. And complex noise is very likely to affect the accuracy of detection results, resulting in false-positive or false-negative results [11]. To solve these problems, researchers have spent a lot of effort to improve the hardware of PCR detectors, such as utilizing the gas barrier [12] or using the interface cladding technique on chips to reduce the

✉ Weijia Wen
phwen@ust.hk

1 Advanced Materials Thrust, Department of Physics, Hong Kong University of Science and Technology, Guangzhou, 511458, China

2 Earth, Ocean and Atmospheric Sciences Thrust, Department of Physics, Hongkong University of Science and Technology, Guangzhou, 511458, China

3 Department of Physics, Hongkong University of Science and Technology, Hongkong, 999077, China

4 Center for Soft and Living Matter, Institute for Basic Science (IBS), Ulsan 44919, South Korea

generation of bubbles [8]. However, these hardware-based improvements are expensive and increase the difficulty of the chip fabrication [13, 14].

In fact, the effect of complex noises can be reduced as much as possible by powerful algorithms at a lower cost, as long as they do not affect the brightness variation of all areas within chambers. Different analysis methods may produce completely different results for these complicated problems. At present, industry and academia mainly rely on the traditional algorithm that calculates average brightness with predetermined fixed area for PCR Image Analysis [15, 16]. The fixed calculated area pattern makes this method to be less robust if there is complex noise in the selected area, it may dramatically affect the brightness and cause false-positive or false-negative results directly because the complex noise has great randomness in brightness, location, and occurrence time [10, 15]. Actually, with the development of deep neural networks in the field of image processing, many complicated problems such as irregular noise and target recognition, which are hard to be solved by traditional algorithms can be effectively handled now [17, 18]. As a deep neural network with the functions of target recognition and segmentation, Mask R-CNN has been widely used for many fields such as radar image recognition [19], diseases detection [20], and ship detection [21]. But such an effective method has not been introduced into the field of noise recognition for real-time PCR. Therefore, we proposed a novel Dynamic Deep Learning Noise Elimination Method (DIPLOID) in this paper. Our new method is based on Mask R-CNN and dynamic optimal area selection algorithm (DANA). DIPLOID could automatically recognize and eliminate complicated noises and dynamically select the optimal calculating region.

With the growing problems such as infectious diseases and environmental pollution, the importance of POC devices is daily increasing. It has great application potential for areas such as isolation facilities, customs, and reservoir [22–24]. And accuracy is one of the most important requirements of POC devices. DIPLOID would identify impurities by Mask R-CNN first, then remove impurities and use threshold segmentation to select the preliminary affected area by DANA algorithm, and finally used dynamic programming to select the largest continuous area to calculate the average brightness. With these measurements, DIPLOID could significantly increase the accuracy for experiment images that own impurity interference. As shown in the experiments of this paper, our method increased the accuracy from 57.9 to 94.6% compared with the traditional method. Besides, it decreased the False Positive Rate (FPR) from 34.1 to 4.8% and reduced the False Negative Rate (FNR) from 50.9 to 6.1%, respectively. Compared with the traditional algorithm, the performance improvement of our method is very significant. In addition, our method is more sensitive to brightness variety and more robust to noise interference. So it can improve the accuracy of POC real-time PCR, and make the portable PCR a broader application prospect.

Materials and methods

Materials

Data preparation

In this study, we tested the performance of our method using the standard pathogen RNA sample (COVID-19) and real DNA sample (*Escherichia coli* ATCC 8739). COVID-19 Nucleic Acid Detection Kit (Fluorescent RT-PCR) was purchased from Jiangsu Diagnostics Biotechnology Co Ltd (202103003EN, China). The standard sample, Certified Reference Material of 2019 Novel Corona Virus (2019-nCoV) Ribonucleic Acid Genome (SN:2020-02, GBW(E) 091099, National Institute of Metrology, China) consists of 8.04×10^2 copy/μL E gene, 6.89×10^2 copy/μL ORFlab gene, and 1.36×10^3 copy/μL N gene (Genome coordinate: 1320115600, GenBank No. NC_045512). *Escherichia coli* (ATCC 8739) was originally obtained from Guangdong Huankai Microbial Technology Co LTD, and the strain was activated and cultivated with the Lysogeny Broth (LB) medium as the real samples we used. Nucleic acid was extracted from a 1 ml overnight culture by Wizard Genomic DNA Purification Kit (Promega). In this work, the standard RNA sample and real DNA sample were diluted in TE buffer (17890, Thermal Fisher Scientific) on a scale of 500 and 100000 as template nucleic acid. SWM-01 PCR Nucleic Acids Analyzer (SN:202003010EN, Shineway, China) and microfluidic PCR chip (BS-C3-12/ BS-C6-12, Shineway, China) were used for nucleic acid amplification and shown in Fig. 1.

For RNA standard sample, the total reaction volume is 25 μL which consists of 16 μL RT-PCR Buffer Master Mix, 2 μL COVID-19 Reaction Solution, 2 μL RT-PCR Enzyme Mix, and 5 μL 500-fold diluted RNA Reference Material. For DNA real sample, a 25 μL reaction volume containing 12.5 μL TaqManTM Fast Advanced Master Mix (ThermoFisher, USA), 1 μL INVOA Primer F (10 μM), 1 μL INVOA Primer R (10 μM), 0.5 μL INVOA Probe P (10 μM), 5 μL Rnase-free H_2O from *Escherichia coli* (universal) qPCR test kit (Invitrogen), and 5 μL diluted *Escherichia coli* (ATCC 8739) DNA. Then, 12 μL mixture was independently loaded in the microchip with bubbles that easily be generated by the air-containing pipette tip. According to the users' manual of SWM-01, we set up the following conditions for thermal cycling of COVID-19 RNA standard sample: (1) Reverse transcription: 50 °C

for 15 min; (2) pre-cycle: 95 °C for 3 min; (3) 45 thermal cycles: 95 °C for 10 s and 60 °C for 40 s, with a total reaction time of 55.5 min; and *Escherichia coli* (ATCC 8739) DNA sample according to the following conditions: (1) pre-cycle: 95 °C for 3 min; (2) 45 thermal cycles: 95 °C for 10 s and 55 °C for 40 s, with a total reaction time of 40.5 min. Through the excitation of the blue LED (470nm), the fluorescent images were collected by complementary the metal oxide semiconductor (CMOS) with the resolution of 800 × 480 pixels. It should be noted that the DIPLOID image analysis method proposed in this paper has universal validity, and the types of experiment samples do not affect the effectiveness of the algorithm because they have the same luminescence mechanism.

Dataset and dataset augmentation

Deep learning networks have achieved great success in visual recognition fields such as autonomous driving and face recognition, but one of the most serious limitations for deep learning is the lack of data [25]. The requirement of the large dataset limits the application of deep learning networks in many fields that data is expensive or hard to obtain. To solve this dilemma, deep learning networks based on the small dataset with effective data augmentation methods are becoming more and more popular recently [26, 27]. Because of the high cost to acquire PCR images, we adopted the randomly targets copy strategy [28] combines with the image rotation method [29] as the data augmentation method in this paper. We first randomly copied and pasted impurities with different brightness and size to augment the images, then doubled all data again by rotating them 180°.

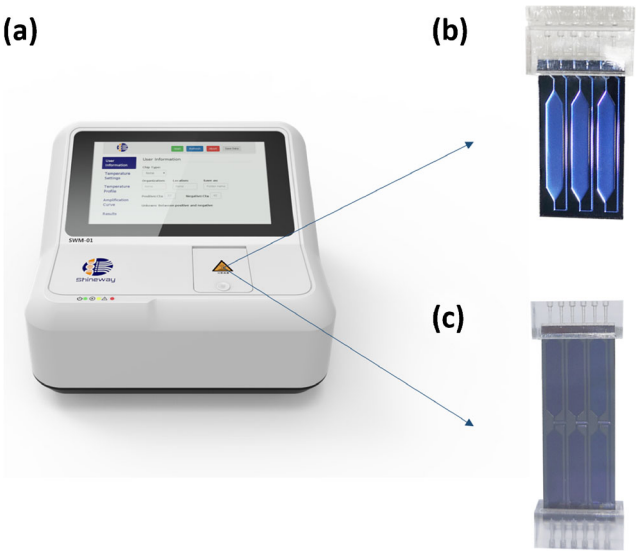

Fig. 1 The testing equipment of portable real-time PCR and microfluid chips. (a) Portable fast microchip PCR analyser of Shineway. (b) 3-chamber chip. (c) 6-chamber chip

This step not only quickly increased the number of training images but also simulated more patterns of noise, which could improve the training efficiency of the model.

The original training dataset contains 450 images, the validation dataset contains 50 images, and the testing dataset contains 1350 images. After augmentation, the original training images were increased from 450 to 1800. The dataset is labeled with polygon box by via-2.0.10, and all annotation information of the training dataset and the testing dataset is stored in two JSON files named VIA_REGION_DATA respectively. We could divide the prediction results into four types: False Negative (FN), True Negative (TN), False Positive (TP), and True Positive (TP). The key factors which present the precision of the prediction results are False Positive Rate (FPR), False Negative Rate (FNR), and Accuracy (ACC) [30–32]: $FNR = FN/(TP + FN)$, $FPR = FP/(FP + TN)$, $ACC = (TN + TP)/(TN + TP + FN + FP)$, $sensitivity = TP/(TP + FN)$, $specificity = TN/(FP + TN)$. The dataset of the current study is available from the corresponding author on reasonable request.

Methods

Methods overview

In this paper, a novel dynamic deep learning noise elimination method based on Mask R-CNN and dynamic selection is proposed as Fig. 2 shows. The DIPLOID could be mainly divided into two parts: interference identification and dynamic selection, which are processed by Mask R-CNN and DANA respectively. First, the Mask R-CNN will identify impurities and output masks for the input images. The ground truth we used to train Mask R-CNN is the manually labeled bubbles and noise. The output of the Mask R-CNN is the recognition result and the mask of impurities, which are shown in Fig. 2(B) and (C) respectively.

Second, the DANA will subtract the impurity regions from original images through the cv2.subtract function. The input image shown in Fig. 2(A) is used as the minuend, and the mask is used as the subtrahend. After subtractions, the gray value of the original corresponding impurity area is perfectly reduced to 0, and pixels in other areas are retained at their original values, and the subtraction result is shown in Fig. 2(D).

Third, the DANA will calculate the Maximum Valid Contiguous Area (MVCA) from the subtraction result. DANA will construct a dynamic programming list (DP) for realizing this task. The subtraction result is binarized by the dynamic selection method with the background mean value as the threshold. The pixels below the threshold are set to 0, and the pixels above the threshold are set to 1.

Fourth, the dynamic selection method is used to calculate the maximum square (Fig. 2(G)) with all values of 1 for

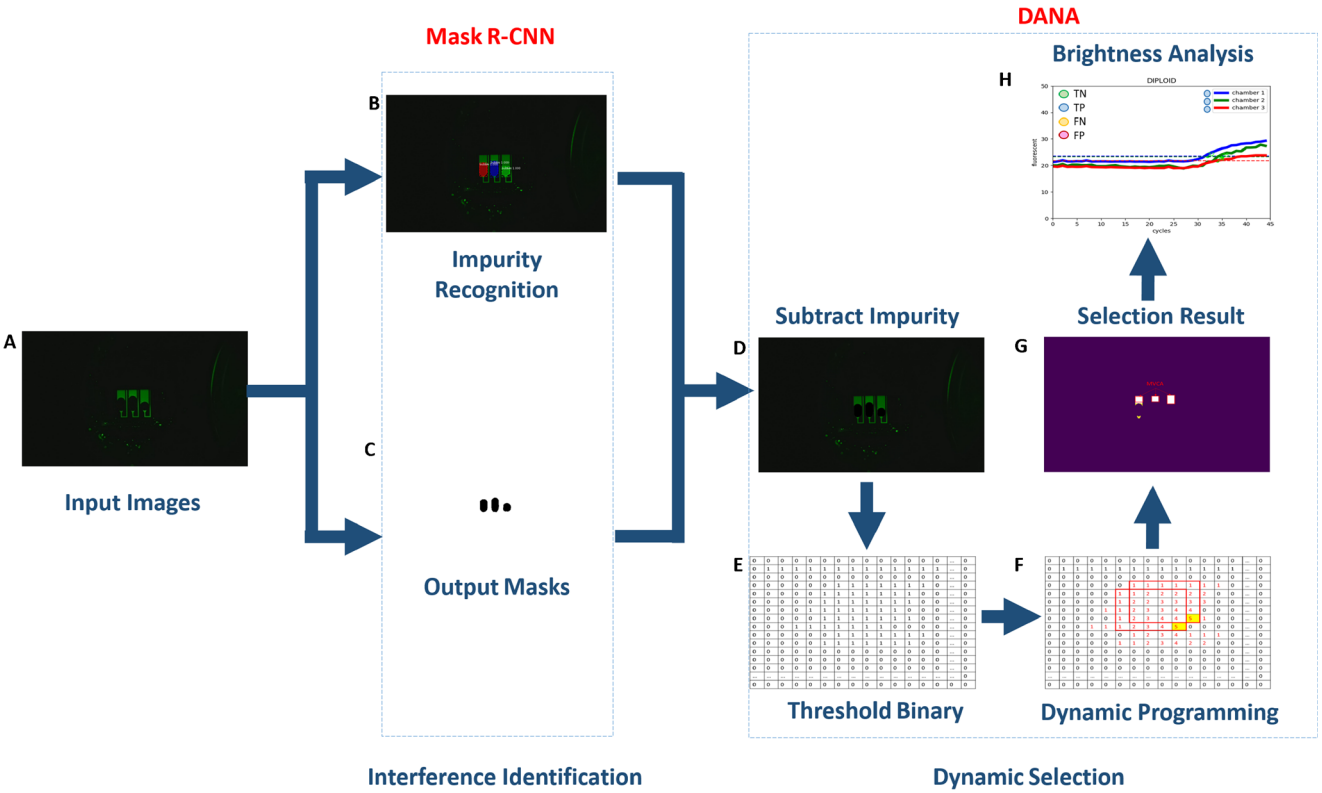

Fig. 2 Flow chart of the processing procedure for DIPLOID. (A) Input images. (B) Recognition result of Mask R-CNN. (C) Output mask. (D) Subtraction result. (E) Threshold binary result. (F) Dynamic programming result. (G) MVCA result. (H) Brightness analysis of MVCA

calculating the brightness curve. According to the dynamically selected region, the average gray value in the region is calculated and the brightness change curve is output to make predictions (Fig. 2(H)), where the x-axis of the curve is the cycle number and the y-axis is the brightness value.

Last but not least, the cycle threshold (CT) values are used to predict the results of curves, which is the most commonly used method at present [33]. For CT values, it is the x-axis value of the intersection point between the brightness curve and a straights line $y = 10 * std + C_3$, where C_3 is the brightness value of cycle 3 and the std is the standard deviation from cycle 3 to cycle 15. After calculating the intersection point (x_i, y_i) between the brightness curve and the straight line, if $x_i \leq 37$ then the prediction is positive, if $x_i \geq 40$ then the prediction is negative, and if $37 < x_i < 40$ then the prediction is unknown and need to be tested again.

Mask R-CNN

Mask R-CNN plays an important role in DIPLOID for identifying the location of bubbles and noise, its recognition result will directly affect the selection effect of DANA. Since the bubbles and noises themselves have initial brightness and are easily adherent with each other in the liquid region, it is difficult to remove them directly by the traditional algorithm, so we introduce Mask R-CNN which is more accurate in region segmentation. Since Mask R-CNN uses ROI Align instead of ROI Pooling on the basis of Fast R-CNN, so it can locate the target spatial location more accurately. The structure and parameters of the model we use in this paper are shown in Fig. S1 and Table S1, respectively. Mask R-CNN expands the function of predicting segmentation masks based on Fast R-CNN, so it will output masks for each ROI, which provides a design basis for interference elimination of DIPLOID. DIPLOID uses Mask R-CNN to identify interfering objects in the input image and output Mask. Thus, DIPLOID can accurately eliminate the noise region and make its gray value to be accurately identified as 0 in the subsequent dynamic programming, which is one of the cores of our proposed method.

Compared with other instance segmentation algorithms that first divide then classify, Mask R-CNN adopts a three-way parallel design conception, which can synchronize the classification and segmentation operation, making the network simpler and more efficient. The loss of Mask R-CNN is defined as $L = L_{cls} + L_{box} + L_{mask}$, in which the L_{cls}, L_{box}, and L_{mask} represent the classification loss, bounding-box loss, and average binary cross-entropy loss respectively [34].

DANA

The new PCR image detection method, DIPLOID, that we propose in this paper can be mainly divided into two parts: interference identification (by Mask R-CNN) and dynamic selection (by DANA). Successful noise identification by the deep neural network is only the first step. To effectively select the optimal region, we also need an effective dynamic selection algorithm. Therefore, in this section, we proposed a novel dynamic optimal area selection algorithm (DANA) to achieve fully automatic selection according to the features of real-time PCR images.

DANA will first store the original images and masks of interference produced by Mask R-CNN under the same path, where the masks are named according to the format of image name + number. Then, classify them into the corresponding sub-directories according to the number of cycles and naming rules, then perform the cv2.subtraction operation among the image and masks in each sub-directory. When subtrahend is the mask format, cv2.subtract will only keep the pixels of the input image which correspond to the non-zero area of the mask, and all the other pixels are uniformly cleared to 0. So before operating subtractions, we first need to apply an invert operation for the mask which is output from Mask R-CNN, to make the regions of impurities are 0 and the other pixels are 1.

Second, DANA will adopt the distinguish threshold which is calculated by the background mean value to recalculate the subtraction results into binary format, where the pixels with a luminance below the threshold are considered as 0 while the pixels with a luminance above the threshold are considered as 1. The value of the distinguish threshold can be decided either by the average background brightness or manual adjustment. For example, if the background area is $[x_1 : x_2, y_1 : y_2]$, and the total number of pixels among this area is N, the $threshold = \sum_{x=x_1,y=y_1}^{x=x_2,y=y_2}(R*0.3+G*0.59+B*0.11)/N$, where the R, G, and B represent the value of 3 channels for each pixel.

Then, DANA will compute the Maximum Valid Contiguous Area (MVCA) from all effective areas with the pixel value of 1 and the MVCA will be used for the brightness analysis. During the process of computing MVCA, we need to construct a dynamic programming list (DP) to select the optimal area effectively as Fig. 2(G) shows. The initial input is the binarized image after the threshold prediction process as Fig. 2(E) shows. As for Fig. 2(F), it will update the values in Fig. 2(E) according to the formula (1), where *i* represents the number of rows and *j* represents the number of columns. Roughly speaking, the first row, first column, and all pixels with the value of 0 will keep their original values, and other pixels will be calculated iteratively from left to right and from top to bottom in a group of four points as green boxes in Fig.S2(b) shows. The calculation method for each box is to update the value of the bottom-right point as the minimum value among these four points plus one except the bottom-right value is 0. After all iterations are completed, the maximum value stored in the new DP is the edge length of the MVCA, and the corresponding point DP[i][j] is the bottom-right point of the MVCA as the yellow box in Fig.S2(b) shows. And for the following formulas: the L_{MVCA} represents the length of the MVCA, (x_1, y_1) and (x_2, y_2) represent the upper-left and bottom-right points of the MVCA, respectively.

$$DP[i][j] = \begin{cases} DP[i][j] & i = 0 \; or \; j = 0 \\ 0 & DP[i][j] = 0 \\ min(DP[i-1][j], DP[i][j-1], & \\ DP[i-1][j-1]) + 1 & otherwise \end{cases} \tag{1}$$

$$L_{MVCA} = max(L_{MVCA}\ ,\ DP[i][j]) \tag{2}$$

$$(x_2, y_2) = (i, j)_{DP_{max}} \tag{3}$$

$$x_1 = (x_2 + 1) - L_{MVCA} \tag{4}$$

$$y_1 = (y_2 + 1) - L_{MVCA} \tag{5}$$

Finally, the MVCA will be the selected areas for brightness analysis. The calculation method for brightness analysis is the same as the traditional algorithm, where the histograms of all pixels in the MCVA are summed and averaged, then save and output by different chambers and make the prediction for each chamber.

Comparative methods and training environment

We adopted the most commonly used traditional fixed selection algorithm and the human selection method as comparative methods in this paper. The traditional fixed selection algorithm is selected as the ground truth method because it is one of the most commonly used methods for qPCR in the industry at present. For this method, it usually needs to manually predetermine an effective region as the brightness calculation region for each chamber according to the size and structure of the chip. This region is usually rectangular and contains the entire reaction chamber, which does not change during the subsequent cycle. In industrial production, the regions are usually measured and set in advance by the equipment manufacturer. Besides, the regions need to be manually redefined if there are any changes in the chip design. As the most commonly used method, the fixed selection method only works efficiently for images with uniform brightness. The actual experiments are easily be influenced by uneven heating, impurities, and improper operations, the traditional method is less effective for these complicated situations and may even cause false results. On the

contrary, the human selection algorithm will perform better for these complicated situations. The human selection method manually selected the effective area for each cycle so this area could flexibly vary according to the situation. The human selection method can accurately avoid bubbles, noise, light spots, and other interference, but it is only suitable for laboratory calibration reference since it is quite time-consuming, which can not meet the needs of industrial production.

The training of deep neural networks requires the high performance of computer configuration, so we use the PG620-P2G deep learning workstation with Intel Core I7-9800X processor with the Graphic Card of GeForce RTX 2080 Ti which possesses 11G graphic memory to train the model. Because interference prediction and dynamic selection require lower arithmetic power. Considering the practicality so we used Precision 5820 which owns the processor of intel Xeon W-2245 for processing the DIPLOID. The project is installed on anaconda3-4.4.0 of Linux system with python 3.6 and OpenCV2, and the TensorFlow (TensorFlow-gpu 1.9.0) and Keras (Keras-applications-1.0.8) are also installed in the virtual environment of the anaconda.

Results and discussion

Results of solving false-negative problem

The bubble is one of the most severe challenges during PCR reactions, which can easily cause false-negative results. The bubbles will greatly reduce the fluorescence brightness of the covered area. The traditional method usually selects the whole chamber or a fixed area during the entire reaction period and is therefore susceptible to false-negative results from bubbles when they cover a large area.

As the experiment is shown in Fig. 3, the reactants of chambers 1 to 3 are standard samples, so the theoretical results should all be positive with an exponential growth trend. However, due to the large bubble area in chambers 2 and 3, the average regional brightness is seriously affected. If the traditional algorithm is adopted, as shown in Fig. 3(d), the brightness of chambers 2 and 3 is seriously lowered by the bubble region, thus presenting false-negative results with the flat trend. On the contrary, the effect of bubbles on brightness is minimized since DIPLOID is able to recognize and avoid the bubble region. Its analytical results are shown in Fig. 3(f), where all three chambers are correctly predicted to be positive with a clear exponential growth trend. Human selection is another commonly used method in laboratory studies, but this method is highly dependent on experience and time-consuming. However, our method is fully automated, time-saving, and more suitable for commercial and research purposes.

As the performance analysis is shown in Fig. 4, the traditional method is easily affected by bubbles, with the accuracy of less than 40% and the false-negative rate of higher than 60%. While the accuracy of DIPLOID is 100%. When dealing with the problem of bubbles, the performance of DIPLOID far exceeds the traditional method.

Results of solving the false-positive problem

Complicated noise is another factor that seriously affects accuracy because it may lead to a false-positive result. Complicated noise of real-time PCR has features such as high brightness, irregularity, and overlap with the reaction area. As the example is shown in Fig. 5, the complex noise is difficult to be removed by the traditional method. In this experiment, we used the negative control in chambers 2 and 3, and *Escherichia coli* (ATCC 8739) in chamber 1. So, the theoretical analysis results of chamber 1 should be positive, and results of chambers 2 and 3 should be negative. However, the bubble and complicated noise were observed in chamber 1 and chamber 2, respectively. The cause of these problems may because of the pollution of reaction liquid, the noise of light source, or unregulated operation.

For this situation, since the effective region in chamber 2 is changing all the time, human selection needs to repeatedly measure and calibrate the target region for each cycle, which is cumbersome and time-consuming. And if the traditional method is adopted, it mistakenly counts the noise brightness change into the effective region and wrongly outputs the positive growth trend as chamber 2 of Fig. 5(d) shows, and it also incorrectly predicts the chamber 1 to be negative with the influence of the bubble. On the contrary, the DIPLOID removed the noise and bubbles in the impurity subtract step, so it could accurately select the effective undisturbed region and output the negative result for chamber 2 and positive result for chamber 1 as Fig. 5(f) shows, which owns optimal accuracy and conciseness.

As the performance analysis shown in Fig. 6, the traditional algorithm is easy to be influenced by the presence of complex noise because it may wrongly regard the noise brightness as an increase of reactant brightness. So, for the example shown in this section, the traditional method owns the false-positive rate and false-negative rate of more than 30%, and the accuracy of less than 35%. And the DIPLOID has accuracy as high as 100% without false-positive prediction. So, our method is obviously more resistant to complex noise than the traditional method because of the higher detection accuracy and lower false-positive rate.

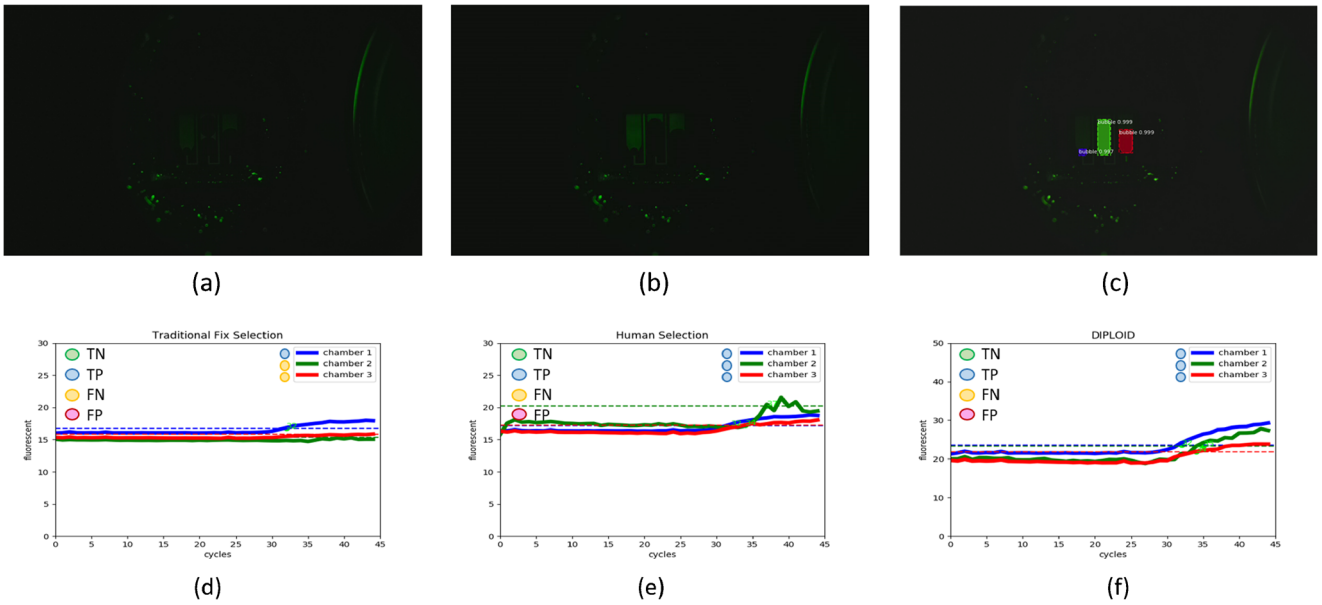

Fig. 3 Original bubble images and comparison results of three different analysis methods. (a) Cycle = 1. (b) Cycle = 45. (c) Bubble detection result by Mask R-CNN. (d) Traditional method. (e) Human selection method. (f) DIPLOID. The blue curve represents Chamber 1, the green curve represents Chamber 2, and the red curve represents Chamber 3. The circle next to the chamber legend represents the prediction result of each Chamber. In (d), Chamber 1 is True Positive (TP), Chamber 2 and 3 are False Negative (FN). In (e) and (f), Chamber1,2,3 are all True Positive (TP)

Discussion

Table 1 presents a comprehensive analysis of the test dataset for three methods, which contains a total of 108 samples, and each of the samples has 45 cycles. We adopted the cross-validation strategy by randomly selecting 48 samples each time and repeating this step five times, then calculating the average value and standard deviation to make the final predictions. In Table 1, the sensitivity represents the probability that positive samples are correctly predicted, and specificity represents the probability that negative samples are correctly predicted [35]. The average sensitivity and specificity of the traditional method were only 49.1% ± 3.3% and 65.9% ± 3.7% respectively, which means the average false detection rate was over 40%. With such a high false detection rate, it is obvious that the traditional method cannot get reliable results under the interference of complex noise. On the contrary, the DIPLOID proposed in this paper showed excellent robustness to interference. Compared with the traditional method, DIPLOID increased the sensitivity and specificity to 93.9% ± 2.2% and 95.2% ± 1.1%, respectively. So, the average false detection rate was decreased to less than 6%, which far exceeds the performance of the traditional method.

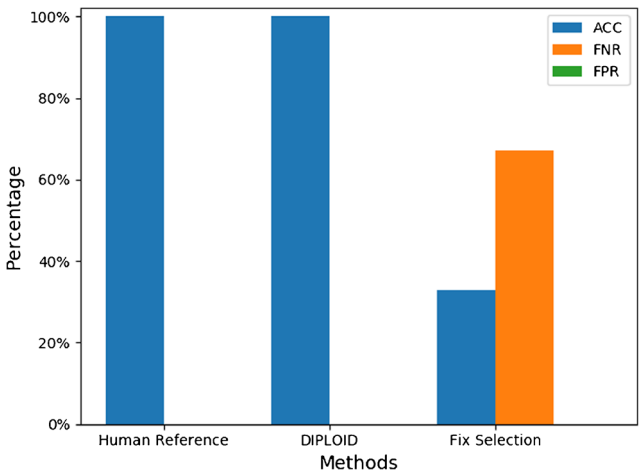

Fig. 4 Performance comparison of the false-negative problem

From the perspective of parameters, the traditional algorithm is similar to the manual selection method. They need 5 key parameters including the x-coordinate and y-coordinate of the start-points and end-points, and the average brightness of the selection area. The parameters of DIPLOID were more complex, Mask R-CNN included 48 major training parameters such as learning rate, steps per epoch, and validation steps. While DANA required 15 major parameters such as DP, MVCA coordinates, and distinguish threshold. The bubble, noise, and background usually have initial brightness for PCR images. Even though some impurities seem to be black, however, their gray values are usually not 0. Therefore, it is difficult to simply find a threshold and separate the interference from the reaction fluid directly. To solve this problem, the DIPLOID method will first accurately identify the precise location of impurities by the deep neural network, then reduce the gray value of the corresponding

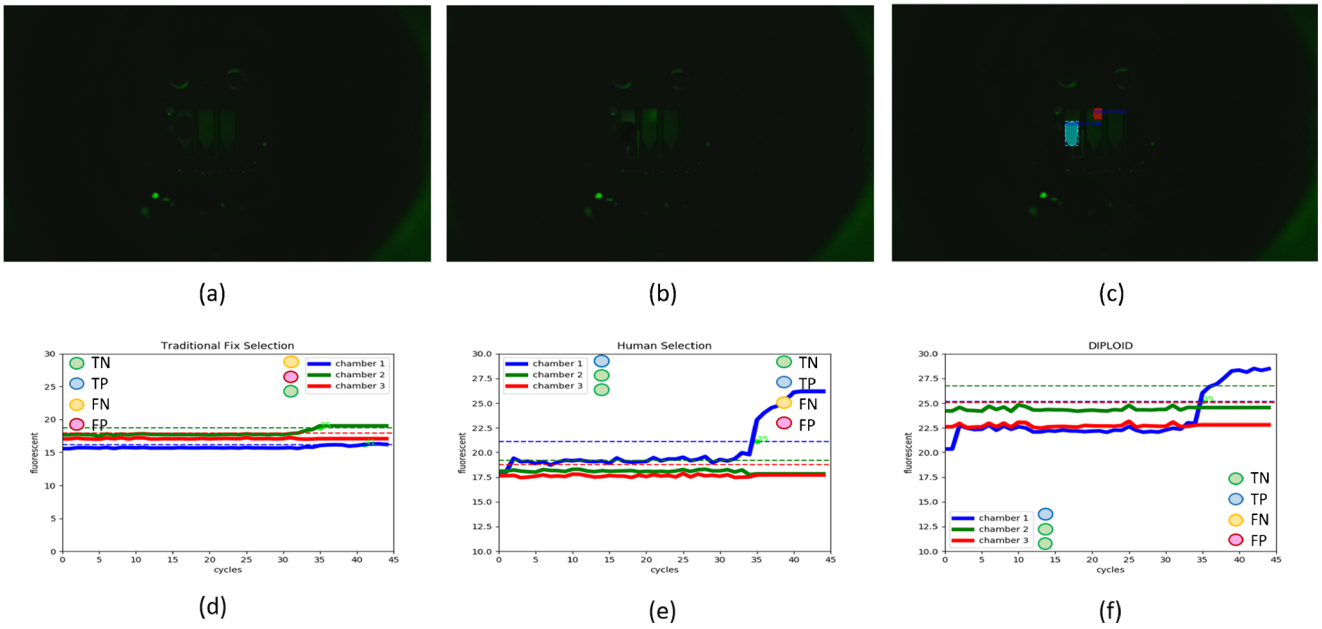

Fig. 5 Original complicated noise images and comparison results of three different analysis methods. (a) Cycle = 1. (b) Cycle = 33. (c) Detection result by Mask R-CNN. (d) Traditional method. (e) Human selection method. (f) DIPLOID. The blue curve represents Chamber 1, the green curve represents Chamber 2, and the red curve represents Chamber 3. The circle next to the Chamber legend represents the prediction result of each Chamber. In (d), Chamber 1 is False Negative (FN), Chamber 2 is False Positive (FP), Chamber 3 is True Negative (TN). In (e) and (f), Chamber 1 is True Positive (TP), Chamber 2 and 3 are True Negative (TN)

area to 0. Therefore, the difference of gray values between the impurity region and reaction fluid region is greatly increased, which makes them much easier to be separated. So, the DANA could calculate the average brightness of the background for separating the MVCA, and the impurity subtraction strategy makes it able to adapt to most samples.

In conclusion, the DIPLOID reaches the state-of-the-art level of PCR image analysis. when dealing with complex noise and bubble problems, the traditional algorithm cannot accurately identify and remove noise due to the inflexible area selection mechanism, and thus shows poor average accuracy as low as 58%. Differently, the DIPLOID improved the average accuracy to 95% by effectively recognizing and removing interference through the deep neural network and maximum area selection algorithm, showing outstanding performance for dealing with complex situations. It is not only sensitive to the brightness change but also more robust to the interference. Compared with traditional algorithms, the DIPLOID algorithm has obvious advantages in accuracy, false-positive rate, and false-negative rate. It can better adapt to the high accuracy requirements of POC real-time PCR, and make the portable PCR have greater potential in future disease detection.

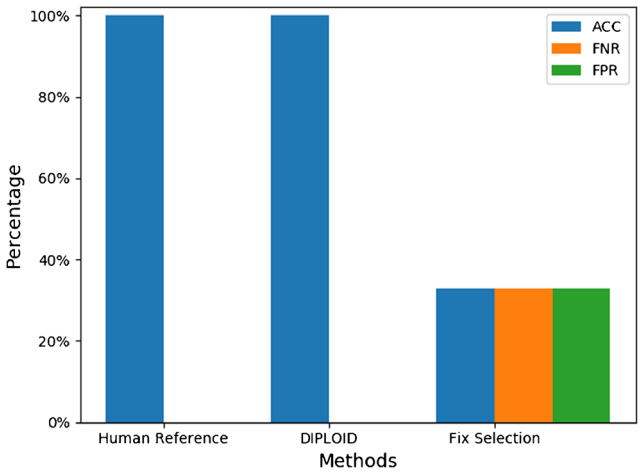

Fig. 6 Performance comparison of the false-positive problem

Table 1 Performance comparison of three analysis methods for test dataset

Method	TP	FP	TN	FN	Sensitivity	Specificity	ACC
Human	23	0	25	0	100.0% ±0.0%	100.0% ±0.0%	100.0% ±0.0%
Traditional	12	8	16	12	49.1% ±3.3%	65.9% ±3.7%	57.9% ±2.7%
DIPLOID	22	1	24	1	93.9% ±2.2%	95.2% ±1.1%	94.6% ±1.1%

Conclusion

POC real-time PCR is becoming one of the most important detection methods for epidemic diseases. The complex noises such as bubbles, fluorescent debris, and light spots influence the accuracy of the real-time PCR hugely. Besides, these problems can easily lead to false-negative or false-positive results. The design of POC PCR usually adopts small volume chambers, which are more likely to produce complex noise. These issues are difficult to be solved by the traditional image analysis method that is widely used now, so we proposed a novel method, DIPLOID, to reduce the influence of the above problems from the aspect of algorithms.

Compared with the traditional fixed selection algorithm, our new method effectively increases the detection accuracy from 57.9 to 94.6%. Besides, because bubbles and complex noise can greatly affect the average brightness, and the traditional algorithm cannot eliminate the interference, so the FPR and FNR of it are up to 34.1% and 50.9%. While the DIPLOID can effectively recognize and eliminate the interference by deep neural network and dynamic selection, so its FPR rate is only 4.8%. After eliminating the interference, the DIPLOID will apply threshold segmentation and then calculate the MVCA, so it is very sensitive to the brightness adjustment and the FNR rate is decreased to 6.1% in our experiments. Our method is more accurate, sensitive, and robust than the traditional method. It can reduce the impact of complex noise as much as possible from the perspective of software, which will allow POC real-time PCR to have more potential in the detection and control of infectious diseases in the future.

Supplementary Information The online version contains supplementary material available at https://doi.org/10.1007/s00216-022-03950-7.

Funding This research was funded by "2019 Shenzhen-Hong Kong Innovation Circle (Category D) (SZST120SC15) (SGDX2019081623160973)", "Zhongshan-HKUST research program (ZSST20SC01)", "Zhuhai Innovation and entrepreneurship team project (ZH01110406180043PWC)", and "the Project of Hetao Shenzhen-Hong Kong Science and Technology Innovation Cooperation Zone (HZQB-KCZYB-2020083)".

Declarations

Conflict of interest The authors declare no competing interests.

References

1. Tahamtan A, Ardebili A. Real-time rt-pcr in covid-19 detection: issues affecting the results. Expert review of molecular diagnostics. 2020;20(5):453–454.
2. Alp A. Advancement in poct molecular testing: the multiplex pcr poct devices for infectious diseases. Ejifcc. 2018;29(3):205.
3. Liu W, Zhang M, Liu X, Sharma A, Ding X. A point-of-need infrared mediated pcr platform with compatible lateral flow strip for hpv detection. Biosens Bioelectron. 2017;96:213–219.
4. Bidmanova S, Kotlanova M, Rataj T, Damborsky J, Trtilek M, Prokop Z. Fluorescence-based biosensor for monitoring of environmental pollutants: from concept to field application. Biosens Bioelectron. 2016;84:97–105.
5. Jung W, Han J, Choi J-W, Ahn CH. Point-of-care testing (poct) diagnostic systems using microfluidic lab-on-a-chip technologies. Microelectron Eng. 2015;132:46–57.
6. Kim H, Chung D-R, Kang M. A new point-of-care test for the diagnosis of infectious diseases based on multiplex lateral flow immunoassays. Analyst. 2019;144(8):2460–2466.
7. Ahrberg CD, Choi JW, Lee JM, Lee KG, Lee SJ, Manz A, Chung BG. Plasmonic heating-based portable digital pcr system. Lab Chip. 2020;20(19):3560–3568.
8. Liu H-B, Gong H-Q, Ramalingam N, Jiang Y, Dai C-C, Hui KM. Micro air bubble formation and its control during polymerase chain reaction (pcr) in polydimethylsiloxane (pdms) microreactors. J Micromech Microeng. 2007;17(10):2055.
9. Hu Z, Fang W, Gou T, Wu W, Hu J, Zhou S, Mu Y. A novel method based on a mask r-cnn model for processing dpcr images. Anal Methods. 2019;11(27):3410–3418.
10. Karlsson JM, Haraldsson T, Laakso S, Virtanen A, Mäki M, Ronan G, Van Der Wijngaart W. Pcr on a pdms-based microchip with integrated bubble removal. In: 2011 16th International Solid-State Sensors, Actuators and Microsystems Conference, IEEE; 2011. p. 2215–2218.
11. Baker M. Microrna profiling: separating signal from noise. Nature methods. 2010;7(9):687–692.
12. Lee SH, Song J, Cho B, Hong S, Hoxha O, Kang T, Kim D, Lee LP. Bubble-free rapid microfluidic pcr. Biosens Bioelectron. 2019;126:725–733.
13. Zhang C, Xing D, Li Y. Micropumps, microvalves, and micromixers within pcr microfluidic chips: advances and trends. Biotechnology advances. 2007;25(5):483–514.
14. Ramalingam N, Liu H-B, Dai C-C, Jiang Y, Wang H, Wang Q, Hui KM, Gong H-Q. Real-time pcr array chip with capillary-driven sample loading and reactor sealing for point-of-care applications. Biomedical microdevices. 2009;11(5):1007–1020.
15. Orlando C, Sestini R, Zentilin L, Gelmini S, Pinzani P, Giacca M, Pazzagli M. Image analysis in quantitative pcr. an application for the measurement of c-erbb-2 oncogene amplification in dna from human tumours. Journal of bioluminescence and chemiluminescence. 1994;9(3):223–228.
16. Larionov A, Krause A, Miller W. A standard curve based method for relative real time pcr data processing. BMC bioinformatics. 2005;6(1):1–16.
17. Koziarski M, Cyganek B. Image recognition with deep neural networks in presence of noise–dealing with and taking advantage of distortions. Integrated Computer-Aided Engineering. 2017;24(4):337–349.
18. Tian C, Fei L, Zheng W, Xu Y, Zuo W, Lin C-W. Deep learning on image denoising: An overview. 2020. Neural Netw.
19. Qian Y, Liu Q, Zhu H, Fan H, Du B, Liu S. Mask r-cnn for object detection in multitemporal sar images. In: 2019 10th International Workshop on the Analysis of Multitemporal Remote Sensing Images (MultiTemp), IEEE; 2019. p. 1–4.
20. Anantharaman R, Velazquez M, Lee Y. Utilizing mask r-cnn for detection and segmentation of oral diseases. In: 2018 IEEE International Conference on Bioinformatics and Biomedicine (BIBM), IEEE; 2018. p. 2197–2204.
21. Nie X, Duan M, Ding H, Hu B, Wong EK. Attention mask r-cnn for ship detection and segmentation from remote sensing images. IEEE Access. 2020;8:9325–9334.

22. Luppa PB, Müller C, Schlichtiger A, Schlebusch H. Point-of-care testing (poct): Current techniques and future perspectives. TrAC Trends Anal Chem. 2011;30(6):887–898.
23. Valtonen M, Waris M, Vuorinen T, Eerola E, Hakanen AJ, Mjosund K, Grönroos W, Heinonen OJ, Ruuskanen O. Common cold in team finland during 2018 winter olympic games (pyeongchang): epidemiology, diagnosis including molecular point-of-care testing (poct) and treatment. British journal of sports medicine. 2019;53(17):1093–1098.
24. Gomes HIAS, Sales MGF. Development of paper-based color test-strip for drug detection in aquatic environment: application to oxytetracycline. Biosens Bioelectron. 2015;65:54–61.
25. Ma B, Wei X, Liu C, Ban X, Huang H, Wang H, Xue W, Wu S, Gao M, Shen Q, et al. Data augmentation in microscopic images for material data mining. npj Computational Materials. 2020;6(1):1–9.
26. Sung F, Yang Y, Zhang L, Xiang T, Torr PHS, Hospedales TM. Learning to compare: Relation network for few-shot learning. In: Proceedings of the IEEE conference on computer vision and pattern recognition; 2018. p. 1199–1208.
27. Oreshkin BN, Rodriguez P, Lacoste A. Tadam: Task dependent adaptive metric for improved few-shot learning. 2018. arXiv:1805.10123.
28. Ghiasi G, Cui Y, Srinivas A, Qian R, Lin T-Y, Cubuk ED, Le QV, Zoph B. Simple copy-paste is a strong data augmentation method for instance segmentation. In: Proceedings of the IEEE/CVF Conference on Computer Vision and Pattern Recognition; 2021. p. 2918–2928.
29. Mikołajczyk A, Grochowski M. Data augmentation for improving deep learning in image classification problem. In: 2018 international interdisciplinary PhD workshop (IIPhDW), IEEE; 2018. p. 117–122.
30. Luo R, Sedlazeck FJ, Lam T-W, Schatz MC. A multi-task convolutional deep neural network for variant calling in single molecule sequencing. Nature communications. 2019;10(1):1–11.
31. Wang Y, Barbacioru C, Hyland F, Xiao W, Hunkapiller KL, Blake J, Chan F, Gonzalez C, Zhang L, Samaha RR. Large scale real-time pcr validation on gene expression measurements from two commercial long-oligonucleotide microarrays. BMC genomics. 2006;7(1):1–16.
32. Lalkhen AG, McCluskey A. Clinical tests: sensitivity and specificity. Continuing education in anaesthesia critical care & pain. 2008;8(6):221–223.
33. Fuller JA, Njenga MK, Bigogo G, Aura B, Ope MO, Nderitu L, Wakhule L, Erdman DD, Breiman RF, Feikin DR. Association of the ct values of real-time pcr of viral upper respiratory tract infection with clinical severity, kenya. Journal of medical virology. 2013;85(5):924–932.
34. Li X, Cheng S. Pedestrian gender detection based on mask r-cnn. In: 2019 IEEE 5th International Conference on Computer and Communications (ICCC); 2019. p. 2082–2086.
35. Bossuyt PM, Reitsma JB, Bruns DE, Gatsonis CA, Glasziou PP, Irwig L, Lijmer JG, Moher D, Rennie D, De Vet HCW, et al. Stard 2015: an updated list of essential items for reporting diagnostic accuracy studies. Clinical chemistry. 2015;61(12):1446–1452.